RESEARCH PAPER

Application of 3D laser scanning on NATM tunnel deformation measurement during construction

Yu Zhao[1] · Zhizhong Zhu[1] · Wei Liu[2] · Jianyong Zhan[1] · Dun Wu[3]

Abstract

The 3D laser scanning technology is implemented to multi-temporally scan the lining of a NATM tunnel during construction. An improved moving average method (IMAM) is firstly proposed for downsizing the scanned point clouds. The correspondence between two temporal point clouds is determined by the iterative closest point (ICP) algorithm, and then the deformation between each paired points was obtained throughout the data. Subsequently, the full-space deformation field of tunnel lining can be calculated, which provides extensive deformation information of the complete tunnel lining for construction. The verification is conducted by a 20-mm convergence test, and it shows that the IMA method can maintain the accuracy at 78% when the reserved ratio is as low as 3% in NATM tunnel, which is significantly better than the random sampling method and the curvature sampling method. The results also indicate that proposed deformation analysis method performs well even for rough linings. The validation of the proposed method is carried out by comparing the 3D laser scanning and total station measurement of the Nanshan Tunnel. The measurement using the proposed technology has a good agreement with that obtained by using traditional total station monitoring method. In addition, the full-space deformation field of tunnel lining can be obtained for more extensive discussion on the development of deformation.

✉ Wei Liu
  ggoulmmeng@suda.edu.cn

  Yu Zhao
  zhao_yu@zju.edu.cn

  Zhizhong Zhu
  zzzwork@zju.edu.cn

  Jianyong Zhan
  zhanjy@zju.edu.cn

  Dun Wu
  wudun@popsmart.cn

[1] College of Civil Engineering and Architecture, Zhejiang University, 866 Yuhangtang Rd, Hangzhou 310058, China

[2] School of Urban Rail Transportation, Soochow University, 8 Jixue Rd, Suzhou 215131, China

[3] PopSmart Technology Co., Ltd, Ningbo 315100, China

1 Introduction

In situ stress in surrounding rock usually causes large deformation in mountain tunnels, and the deformation monitoring can provide crucial information for construction and maintaining during the lifetime of a tunnel. The deformation monitoring is essential for guiding construction [3, 10, 12], and the long-term monitoring is necessary for risk management [5, 8].

The traditional tunnel deformation monitoring methods, such as direct measurement by convergence gauge or total station, are performed on a limited number of selected points. These methods are unable to show the comprehensive deformation of tunnel efficiently [11]. Recently, the 3D laser scanning technique which acquires 3D point cloud data that reflect the 3D spatial information [7] has been gradually applied into geometric measurement and deformation observation in geology and engineering [4, 16, 18]. This technique provides an alternative method for tunnel deformation monitoring [21, 24] with advantages

of high efficiency, high precision and non-contact characteristic [9, 13].

The tunnel full-space deformation field refers to the deformation distribution on the surrounding rock mass of the tunnel [20]. Through 3D laser scanning, the full-space deformation field of tunnel can be visualized. The deformation changes at any location can be detected by comparing scan data collected at different time. The 3D laser scanning shows good performance in the deformation monitoring of shield tunneling with smooth lining [17, 22]. However, for the tunnel with rough lining, such as New Austrian tunneling method (NATM) tunnel, it is difficult to identify the corresponding relation among multi-temporal data and to obtain accurate tunnel full-space deformation field from massive point cloud data. In order to obtain the above-mentioned correspondence, Monserrat and Crosetto (2008) created a three-dimensional surface model by using least square method and other surface fitting algorithms, which improves the efficiency of deformation analysis. However, it is likely to lose the detail features of point clouds and causes errors when using this modelling method. Teza et al. [19] proposed a new well-performed method for automatic calculation displacement of landslide based on iterative closet point (ICP) algorithm.

For the NATM tunneling, the deformation field measurement is constrained by the following two limitations: (1) loss of feature information subjected to rough surface of primary lining, resulting in the impropriate determining on the correspondence between the two temporal point clouds; and (2) time-consuming calculation of full-space deformation because of the enormous volume of point cloud data.

In this paper, the 3D laser scanning technique is applied to the deformation monitoring of a NATM tunnel in Wenzhou, Zhejiang Province, China. In Sect. 2, the data acquisition, data downsizing and deformation calculation methods are introduced step by step. In Sect. 3, the verification of the data downsizing method is performed through convergence simulation. In Sect. 4, the full-space deformation field is obtained for the tunnel and a comparison is made between traditional monitoring method with total station and the proposed method in this paper.

2 Methodology

2.1 Data acquisition

In order to obtain high-quality point clouds along the tunnel, the scanning process is divided into multiple steps to collect data of different spans, and thus registration of point clouds in different spans is important. Tunnel point clouds data usually require post-registration with the aid of

a target [25]. The traditional target registration process through identifying the target center may cause large error, up to 4 mm, due to the poor environment in the tunnel [1].

In this section, a Trimble SX10 3D laser scanner (Fig. 1), which can achieve high-precision point-wise measurement, high-speed 3D scanning and photography, is adopted to obtain point clouds. Embedded with the total station measurement function, this scanner can obtain 3D point clouds in the unified coordinate system by resection. As a result, the monitoring efficiency is greatly improved and target registering error is avoided compared to the traditional laser scanning with targets. Measuring speed of Trimble SX10 is 26,600 points per second, and the measuring range can reach 600 m, which meets the monitoring requirements. The specification of the Trimble SX10 is listed in Table 1.

In this paper, the space resection method is adopted to reduce the error in data acquisition process. Figure 2 shows monitoring process using space resection. Two prisms, served as back-view points, are set up on the left and right side, respectively, in the stable area (on the secondary

Fig. 1 Trimble TX 10 laser scanner

Table 1 Parameters of Trimble TX 10

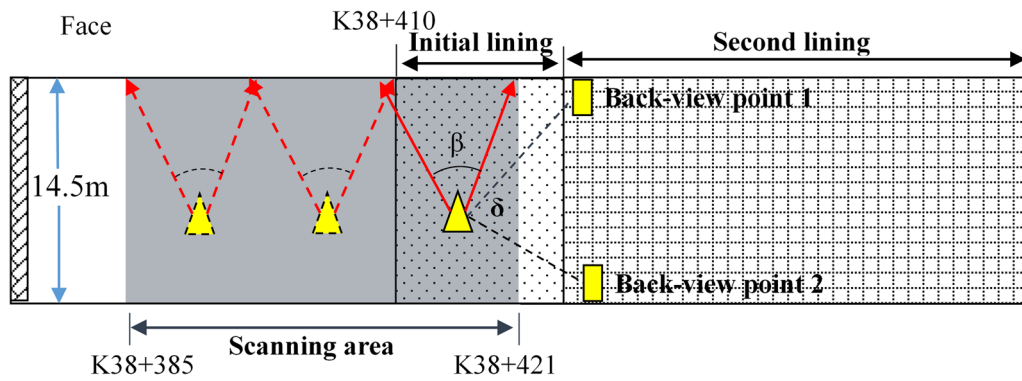| Scanner type	Trimble TX 10
Angel accuracy	1″
Least count	0.1″
Length accuracy	1 mm $\pm$ 1.5 ppm
Speed	26.6 kHz
Point interval	6.25 mm, 12.5 mm, 25 mm, 50 mm @ 50 m
Scope	360° $\times$ 300° (vertical * horizontal)

Fig. 2 The monitoring process using resection method (top view)

lining) (Fig. 2). Before scanning, the coordinates of the two back-view points are gauged by total station. The position of the scanner can be calculated using resection method by observing the prisms using total station incorporated in the Trimble SX10. Therefore, the coordinates of point clouds obtained subsequently are registered in the tunnel coordinate system, which substitutes the target registration. In this way, the coordinates of point clouds obtained at different stations share the same coordinate system when moving the scanner along the tunnel, and the deformation change between multi-temporal point clouds is calculated in the same coordinate system. Accordingly, the accuracy and efficiency of data processing are improved.

The obstacles between the scanner and the lining of the tunnel should be cleared before scanning. As excessive incident angle on the tunnel lining will reduce the measuring accuracy, and the distance between two stations is set as approximately equal to the diameter of the tunnel to ensure β no more than 90°. Furthermore, the angel δ is supposed to be between 30° and 120° to guarantee the accuracy of resection when moving the station. The interval of point cloud is 25 mm @ 50 m, which infer the point cloud interval is 25 mm when the target surface is 50 m away from the scanner.

The raw point clouds contain lots of irrelevant data, and therefore, they need to preprocess before analysis. As shown in Fig. 3, the useless information such as the ground and mechanical devices is manually deleted and the noises points caused by the measured object or measurement system are removed using Gaussian filtering. The preprocessing is carried out with the Geomagic Studio software.

2.2 Data reduction

The large amount of point cloud data will consume lots of computing resources to find the correspondence between two point sets, leading the low calculation efficiency [26]. The moving average method can efficiently denoise the point cloud data and largely reduce the number of points
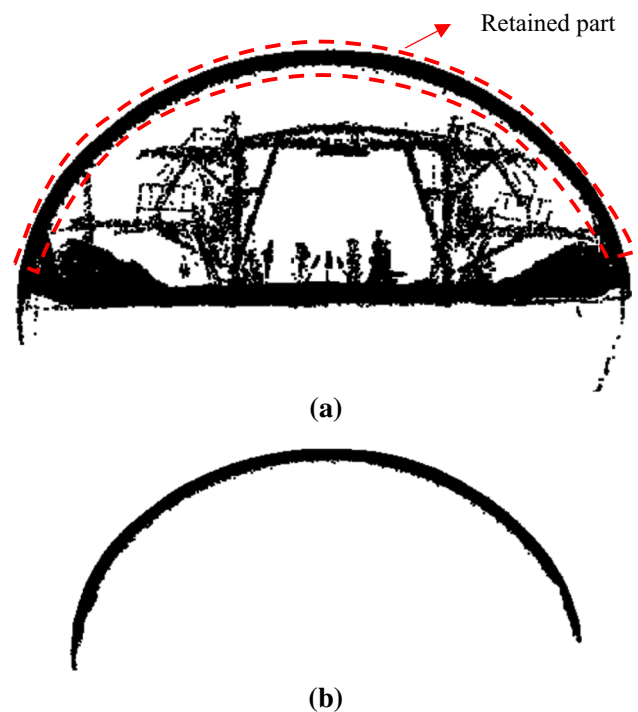

Fig. 3 Preprocessing of removing the noises point cloud. **a** The primitive point cloud. **b** The processed point cloud

while guaranteeing that the most important features are preserved. However, the traditional moving average method based on simple arithmetic mean to extract feature points within the moving window is not suitable for tunnel lining point clouds with curved surface. Therefore, an improved moving average (IMA) method is proposed as follows.

The principle of the proposed method is to replace the observed values with the midpoint value in fitted curved surface within the window. Firstly, a reasonable window length should be set to segment the point cloud data. The moving direction of the window in space is parallel to the *X*, *Y*, *Z* axes in Cartesian coordinate system (Fig. 4), so that the points are regularly distributed in the longitudinal and
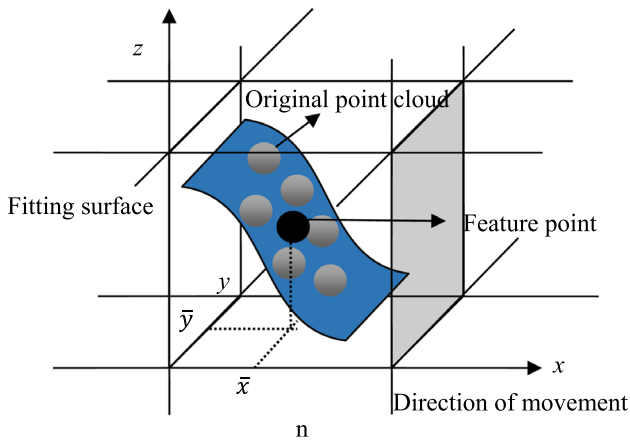
Fig. 4 The diagram of the improved moving average method

lateral directions of the tunnel. The points falling in the window are fitted with a quadric curved surface $z = F(x, y)$, as shown in Eqs. (1). The feature point within the window, namely the center point, is represented as $p_c = (\overline{x_n}, \overline{y_n}, F(\overline{x_n}, \overline{y_n}))$, as shown in Fig. 4, which can be calculated with Eqs. (2) and (3),

$$F(x, y) = ax^2 + by^2 + cx + dy + e \tag{1}$$

$$\overline{x_n} = \sum_i^m \frac{x_i}{m} \quad \overline{y_n} = \sum_i^m \frac{y_i}{m} \tag{2}$$

$$z = F(\overline{x_n}, \overline{y_n}) \tag{3}$$

where m is the number of points within the window and $\overline{x_n}, \overline{y_n}$ is the center of the nth window in the x–y plane.

Through moving the window along the axes by appropriate step (in this paper, the moving step is set as 0.5 times window length) and traversing overall point clouds, the new point cloud data of the tunnel composed of all feature points are generated as shown in Fig. 5. By this improved moving average method, the initial point cloud data are effectively reduced while preserving geometric feature of the tunnel lining, thus ensuring the accuracy of the deformation calculation based on the reduced point clouds.

2.3 Calculation method of tunnel full-space deformation field

As shown in Fig. 6, the calculation of deformation needs to establish the correspondence between points of the two temporal point clouds (point cloud P and point cloud Q), and the point P_i is correspond to Q_i. Therefore, the iterative closet point (ICP) algorithm proposed by Besl and Mckay [2] is used for determining the best corresponding point pairs. Based on the least square method, the ICP algorithm
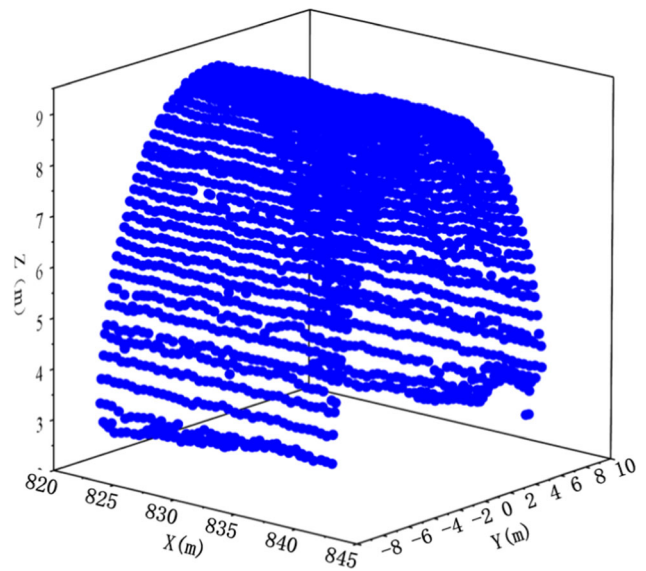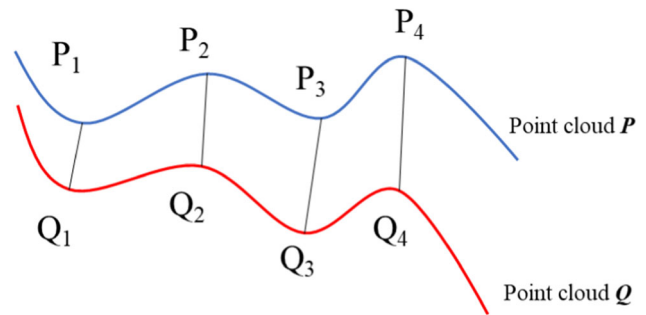

Fig. 5 Tunnel point cloud data after IMA method

Fig. 6 The correspondence between point cloud P and Q

is essentially an optimal matching algorithm calculated by the repeated transformation of rotation and translation. The correspondence between two temporal point clouds is determined in the following part.

Define P_k as the updated P after k times iteration (P_0 is the initial point cloud), and Q_i as the corresponding nearest point in Q to the point P_i in P. The objective function f_k calculated by Euclidean distance between P and Q in the kth iteration is calculated as Eq. (4).

$$f_k(R_k, t_k) == \sum_{i=1}^n \| (R_k P_{(k-1)i} + t_k - Q_i \|^2 \tag{4}$$

where n is the point number of point cloud P, P_{ki} represents the ith point in P_k, R_k represents the rotation matrix, and the t_k denotes the translation vector, as shown in Eq. (5).

As shown in Eq. (6), P updated with R_k and T_k.

$$R_k = \begin{bmatrix} \cos\beta\cos\gamma & \cos\beta\sin\gamma & -\sin\beta \\ -\cos\alpha\sin\gamma - \sin\sin\beta\cos\gamma & \cos\alpha\cos\gamma + \sin\alpha\sin\beta\sin\gamma & \sin\alpha\cos\beta \\ \sin\alpha\sin\gamma + \cos\alpha\sin\beta\cos\gamma & -\sin\alpha\cos\gamma - \cos\alpha\sin\beta\sin\gamma & \cos\alpha\cos\beta \end{bmatrix}_k$$

$$t_k = (t_x\, t_y\, t_z)^T \qquad\qquad (5)$$

$$\mathbf{P}_k = R_k \cdot \mathbf{P}_{k-1} + t_k \qquad (6)$$

In order to improve the recognition accuracy and efficiency, the two temporal point clouds are divided into several segments along the tunnel axis. Using the ICP algorithm, the best correspondence between the two temporal point clouds is obtained, and the spatial deformation field of the tunnel can be calculated by the following steps:

(1) Minimize f_k and obtain R_k and t_k according to Eqs. (4)–(5);
(2) Generate a new point set $\mathbf{P}_k$ with the R_k and t_k according to Eq. (6);
(3) Substitute $\mathbf{P}_{k-1}$ with $\mathbf{P}_k$ in Eq. (4);
(4) Repeat the step 1 to step 3, and the iteration stops when the difference is less than the threshold τ. The criterion for stopping the iteration is:

$$|f_k - f_{k+1}| < \tau \qquad (7)$$

(5) The correspondence between P and Q is determined, and then the deformation d of the tunnel segment can be calculated by comparing their initial spatial coordinates by Eq. (8);

$$d(P_i, Q_i) = \sqrt{\left(x_{(P_i)} - x_{(Q_i)}\right)^2 + \left(y_{(P_i)} - y_{(Q_i)}\right)^2} \qquad (8)$$

(6) Repeat the above procedures in all segments to obtain the deformation field of the whole tunnel.

3 Verification

The IMA method in point cloud processing are validated using a convergence test in this section. A 20-mm radial convergence is set to the original tunnel point cloud data, as shown in Fig. 7. The deformation value calculated from reduced data processed by the IMA method is compared with the true deformation to evaluate the accuracy. For comparison, the original tunnel point cloud data are also reduced to the same quantity by random sampling method and the curvature sampling method [14], respectively. The parameters used in each method are specified in Table 2.

After calculating the deformation of each point, the deformation field is obtained in Fig. 8, and it shows that the deformation distribution by the IMA method achieves the best performance with most points converged at 20 mm (in yellow). The deformation distribution histograms are plotted in Fig. 9 with the normal distribution curve fitting to analyze the dispersion of the deformation field. The mean value of the deformation field μ acquired by the IMA method is closest to the authentic convergence value 20 mm, and the lower standard deviation means the smaller dispersion, which is superior to the other two methods.

Given that the permissible error is ± 3 mm, the displacement between -23 and -17 mm is regarded as accurate. The accurate rate of the displacement obtained by the IMA method, the random sampling method and the curvature sampling method is 88.50%, 84.75% and 84.2%, respectively, which shows that the IMA method is better than the other two at the same reduction ratio. In other words, the IMA method can maintain the main features of deformation field in the process of data reduction.

Clearly, point cloud data cannot be reduced effectively when the reduction ratio is too large, whereas the original features get vague or even lost and the accuracy of deformation field is low when reduction ratio is too small. Therefore, it is necessary to investigate the accuracy of the deformation field under different reduction ratio, which is corresponding to the window size m. The performance of the IMA, random sampling and curvature sampling methods at six reduction ratios is evaluated. The original number of point cloud is 2693622. The calculation parameters are shown in Table 3, and the accuracy of the obtained deformation at different m is illustrated in Fig. 10.

Figure 10 shows that the accuracy rate with respect to the random sampling and curvature sampling methods decreases rapidly with the reservation ratio, and the accuracy rate is below 50% when the reserved ratio is lower than 0.5%. As a result, the distortion of deformation would occur due to the low accuracy rate. It can be inferred that both the random sampling and curvature sampling methods are incapable of tunnel deformation measurement because of the roughness of initial lining especially at low reserved ratio. In contrast, the accuracy rate predicted by the IMA method is higher than 78% when the reserved ratio is 0.5% or higher. In this research, the window size is 85 mm, and the reserved ratio is 2%.
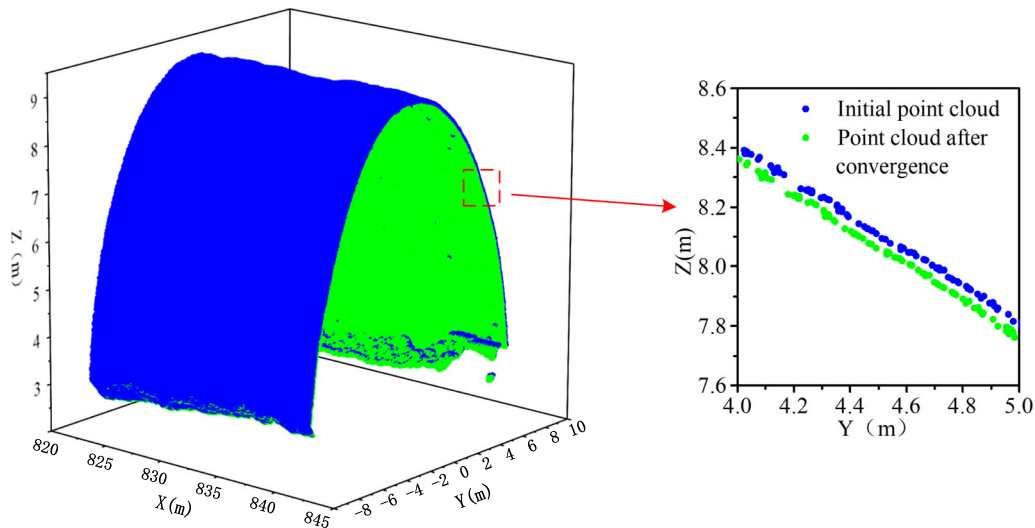
Fig. 7 20 mm convergence test

Table 2 The calculation parameters of the three methods

Method	Random sampling	Curvature sampling	IMA
Sampling ratio/window size	37%	37%	20 mm
Number of original point cloud	2,693,622	2,693,622	2,693,622
Number of point after reduction	999,872	996,640	996,457

4 Cast study

4.1 Project overview

The Nanshan Tunnel as a part of Wenzhou Ring Expressway in Wenzhou, China, contains two paralleled uni-directional three-lane tunnels from K37 + 470 to K38 + 695 (Fig. 11a). The tunnel is 1225 m in length,

14.5 m in diameter and 5 m in height. The section of the tunnel is shown in Fig. 11b.

The Nanshan Tunnel is constructed through the Nanshan Mountain with the highest altitude of about 85 m and the natural slope of about 25°–50°. The depth of cover rock above the tunnel is generally 30–65 m, whereas it is about 5–7 m at the entrance. Silty clay with the thickness of 6 m or less is widely distributed on the top of the mountain. The profile of the surrounding rock is shown in Fig. 11a, and the rock grade determined according to the code [15] is labeled at the bottom. Figure 11a indicates that most of the surrounding rock is Grade IV (Grade V represents the softest rock), which is composed of moderately weathered tuff with catallactic structure. The tunnel is excavated in moderately weathered tuffs with block structures cut by joints. The engineering geological condition is relatively poor for tunneling. Thus, systematic deformation monitoring of the tunnel can provide significant guidance for construction strategy and tunnel safety.

The primary lining has been partly installed in the monitoring area. The composite support structure was used in primary lining, consisting of anchors, steel mesh, steel
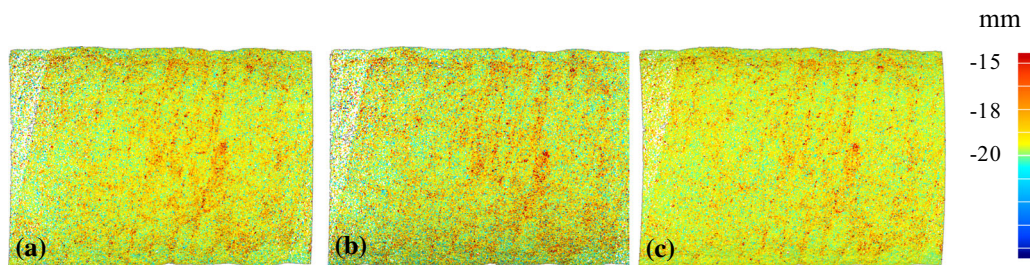

Fig. 8 Tunnel deformation field cloud map. **a** Random sampling method. **b** Curvature sampling method. **c** IMA method
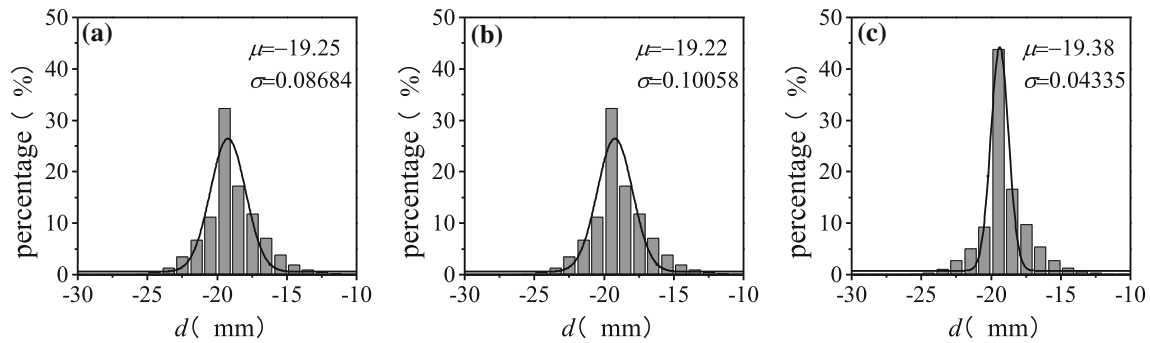
Fig. 9 Deformation distribution histogram **a** random sampling method. **b** Curvature sampling method. **c** IMA method

Table 3 The calculation parameters of IMA

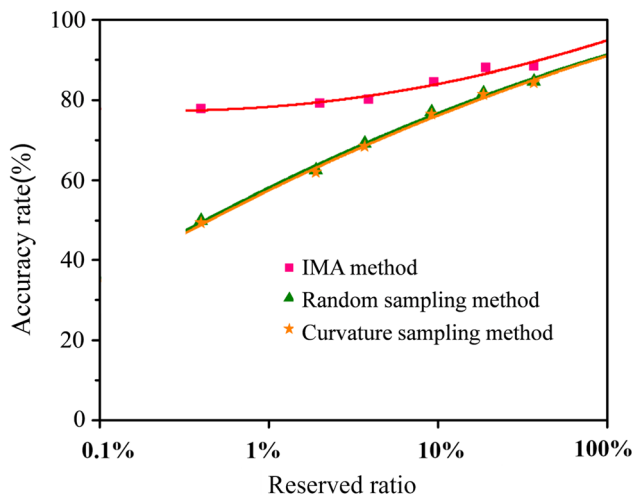| Test	1	2	3	4	5	6
Reserved ratio	40%	20%	10%	5%	2%	0.5%
Window size m in IMA	18 mm	26 mm	38 mm	60 mm	85 mm	180 mm
Number of points	994,625	519,308	254,352	104,563	52,620	11,845

Fig. 10 Deformation accuracy rate versus reserved ratio

arches and sprayed concrete. The secondary lining used 60-cm thick cast in place concrete element, where the deformation became stable.

4.2 Field measurement using 3D laser scanning

Timely deformation monitoring is of great significance to the construction of a NATM tunnel. The deformation monitoring using 3D laser scanning was conducted in the zone between K38 + 385 and K38 + 421 (see Fig. 1), where the rock is rated as Grade IV, and the surface of tunnel is supposed to be cleaned before monitoring. With the tunneling footage of 2 m per day, the tunnel face advanced from K38 + 381 to K38 + 373 in the 4-day

monitoring. In order to observe the deformation of tunnel caused by tunneling, the monitoring is conducted after blasting. The scanning parameters are shown in Table 4.

In order to verify the accuracy of the back-view registration method introduced in Sect. 2.1, the prism coordinates obtained by the laser scanner namely scanned results are compared with the calibration coordinates measured by the total station in Table 5. The test results indicate that the registration error related to the back-view registration method is around 2 mm.

The tunnel point cloud data were collected between section K38 + 385 and section K38 + 421 of the Nanshan Tunnel. Approximately 20 million points were generated. Figures 12 and 13 show the tunnel point cloud data obtained by the 3D laser scanner.

4.3 Result and discussion

The original point cloud data are processed according to the following three steps: (1) data preprocessing; (2) data reduction; and (3) calculation of deformation field. In step 1, irrelevant data except for the tunnel lining surface are eliminated. Noise data subjected to mechanical vibration in the tunnel are reduced by Gaussian filtering [6]. In step 2, the IMA method is employed for data reduction, reducing the number of points from 20 million to 500,000, when the window size in IMA is 85 mm. The point cloud data after the first two steps are shown in Fig. 14. In step 3, the full-space deformation field is obtained with the ICP algorithm.

Based on the ICP algorithm, the deformation fields of three time spans are calculated through comparing the
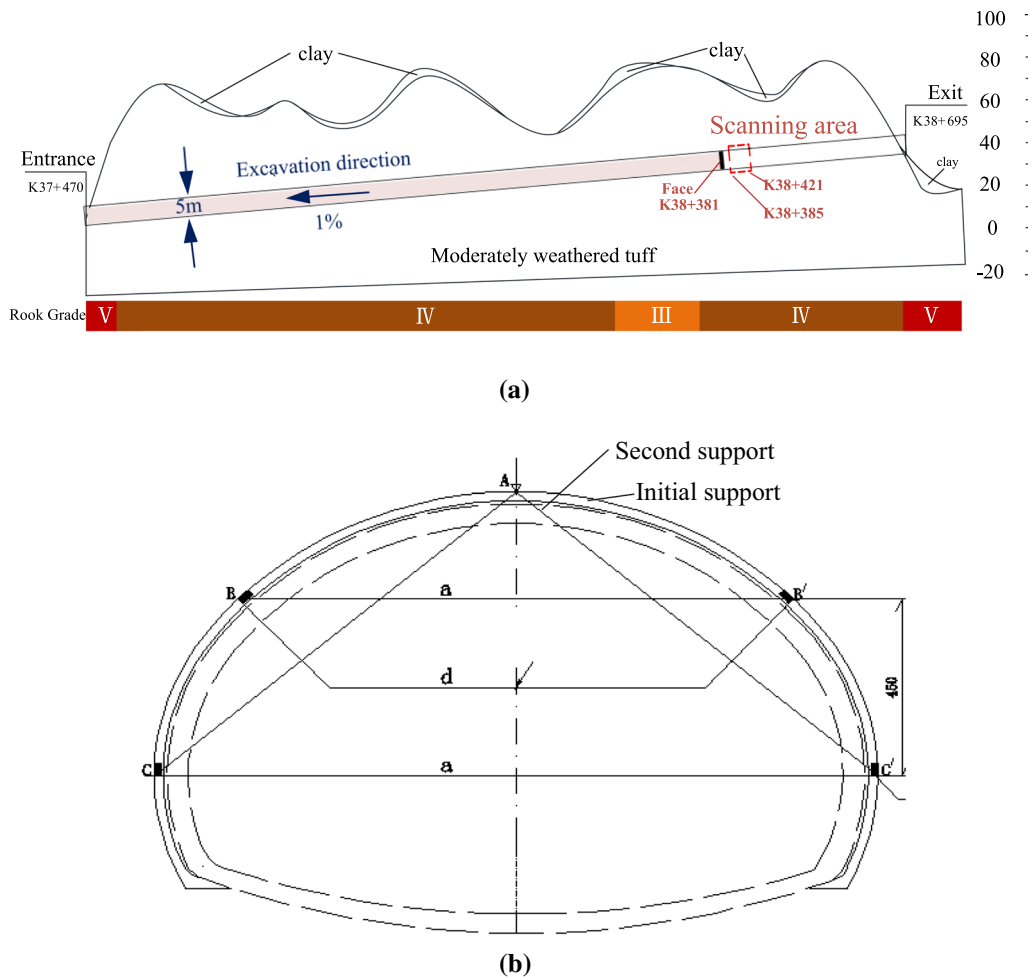
(a)

(b)

Fig. 11 **a** Longitudinal profile of Nanshan tunnel. **b** Section of tunnel

Table 4 Parameters of 3D laser scanning

Parameter	Value
Station distance	15 m
Resection angle δ	30°–120°
Scanning angle β	< 90°
Scanning resolution	25 mm @ 50 m
Single scanning time	15 min

second to the fourth day point cloud data with those of the first day, as illustrated in Fig. 15. The full-space deformation field can provide extensive deformation information of the complete tunnel lining during the construction period. Figure 15 shows that the deformation decreases with the distance from the tunnel face, and the maximum deformation is no greater than 10 mm. For the lining twice the tunnel diameters distance away from the face, the deformation field tends to be stable and less affected by the excavation at the tunnel face.

Table 5 Verification of back-view points measurement

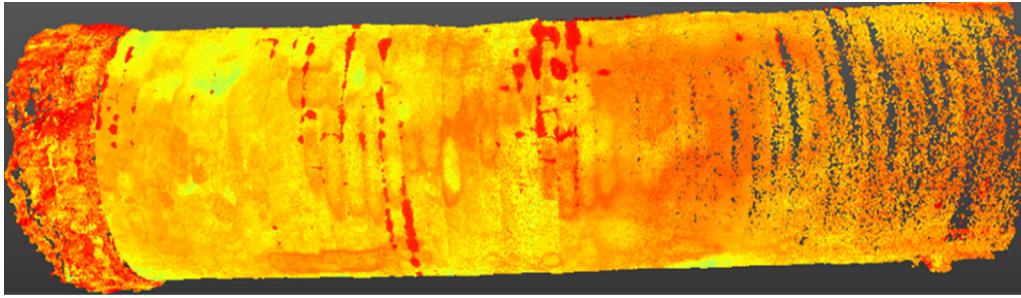| Prism	Calibration results (m)			Scanning results (m)			Error (mm)
	X	Y	Z	X	Y	Z	
1	3,099,538.738	525,836.942	37.685	3,099,538.739	525,836.943	37.686	1.9
2	3,099,551.248	525,852.190	37.718	3,099,551.247	525,852.192	37.719	2.1

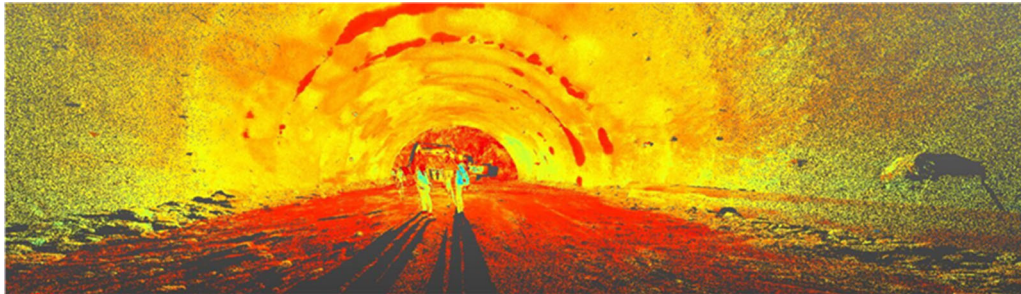**Fig. 12** Tunnel point cloud data (top view, red part indicates lager reflectivity)

Fig. 13 Tunnel point cloud data (inner view)

Fig. 14 Point cloud data after preprocessing

One section is selected every four meters, and then the vault deformation of each section can be obtained for the section-wise deformation comparison. This section deformation is equivalent to the traditional vault deformation obtained with a total station section. Figure 16 compares the deformation of different sections between K38 + 385 and K38 + 421 over different excavation times. The deformation of the primary lining area from K38 + 410 to K38 + 421 is less than 1 mm, indicating that the deformation of these sections is stable, which is consistent with the result of the section convergence measurement. The deformation increases with the excavation time, and the rate of deformation decreases with the distance from the tunnel face. Section K38 + 385, adjacent to the tunnel face, exhibits the highest vault deformation and the steepest increase rate.

The reliability of the 3D laser scanning technology is verified through comparison to traditional total station monitoring method. In the monitoring segment of 3D laser scanning, two traditional monitoring sites were installed at K38 + 395 and K38 + 415, respectively. As illustrated in Fig. 17, the monitoring results by 3D laser scanning are in agreement with the traditional measurement. At the section close to the face, the settlement obtained by 3D laser scanning is slightly larger than that associated with the traditional method. Particularly, the deformation at section K38 + 395 on the second day is 1.6 mm by laser scanning, while it is 1.2 mm acquired through traditional measurement. The difference is inconspicuous at the sections away from the heading. In general, the maximum error is smaller than 0.5 mm, which meets the requirements of field monitoring.

The design of reasonable support system of NATM tunnel relies on the real-time and systematic deformation monitoring data. Thus, compared with the traditional method, the full-space deformation field provided by 3D laser scanning in this paper provides more sufficient information for the design of NATM tunnels. 3D laser scanning is mostly applied in the defamation monitoring of shield tunnels with regular and smooth lining. For shield tunnels, it is easy to determine the deformation by directly compare spatial coordinate along radial direction between two temporal point cloud regardless of the correspondence between them [23], and thus, the density of points is less important. However, due to the rough lining and complicated sections of NATM tunnels, it is incorrect to obtain deformation in the same way. For NATM tunnels, it is necessary to obtain dense point clouds to capture characteristics of the lining, and use the IMA method proposed in
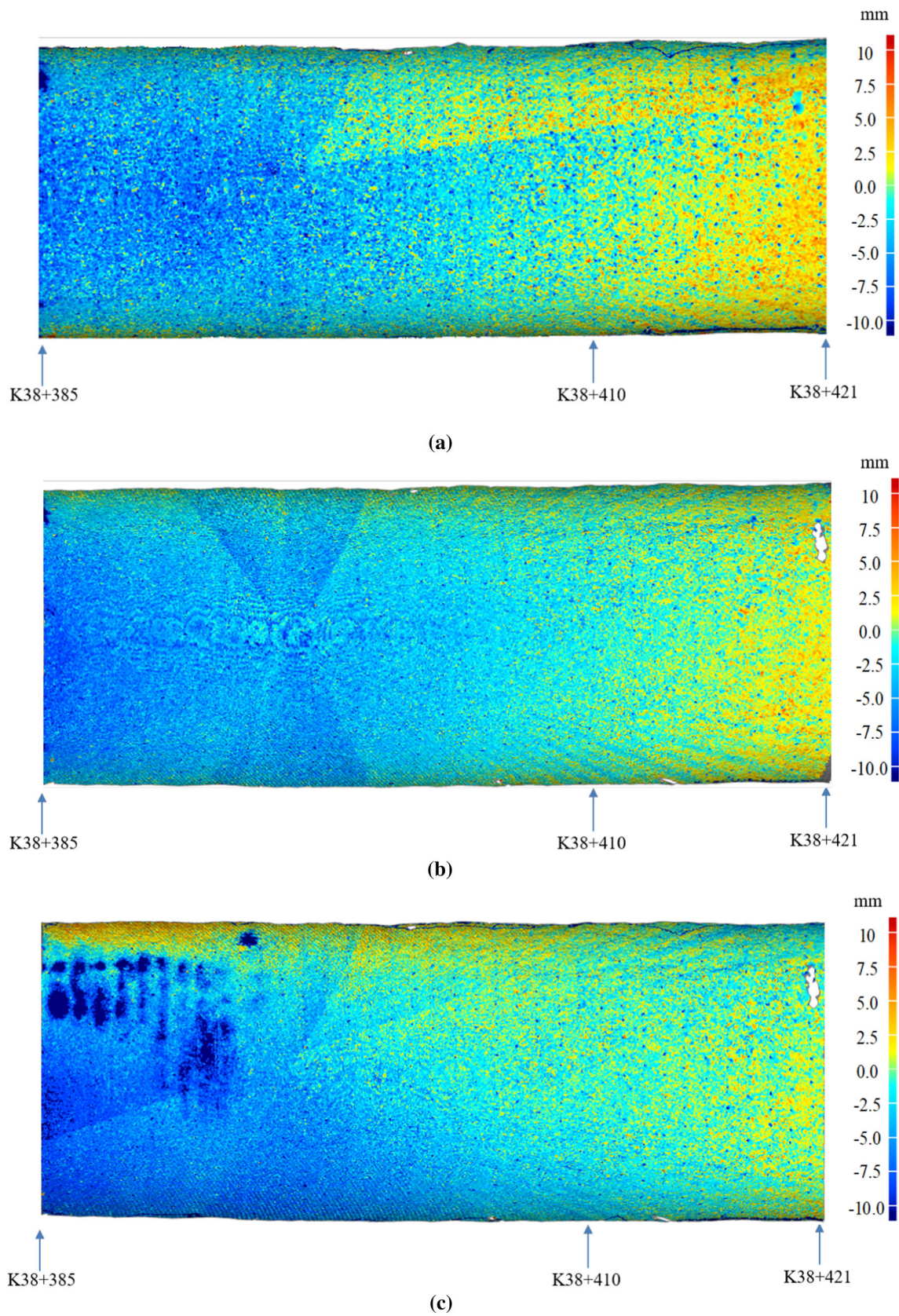
Fig. 15 Tunnel full-space deformation field (top view) **a** deformation between day 2 and day 1, **b** deformation between day 3 and day 1, **c** deformation between day 4 and day 1
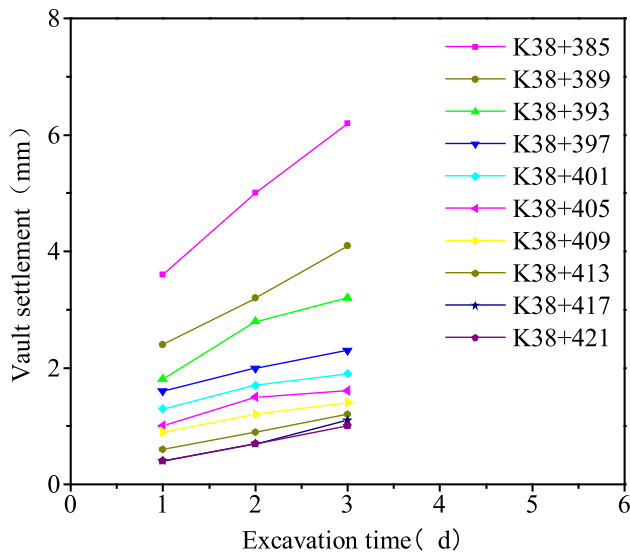
Fig. 16 Vault deformations of sections from K38 + 385 to K38 + 421
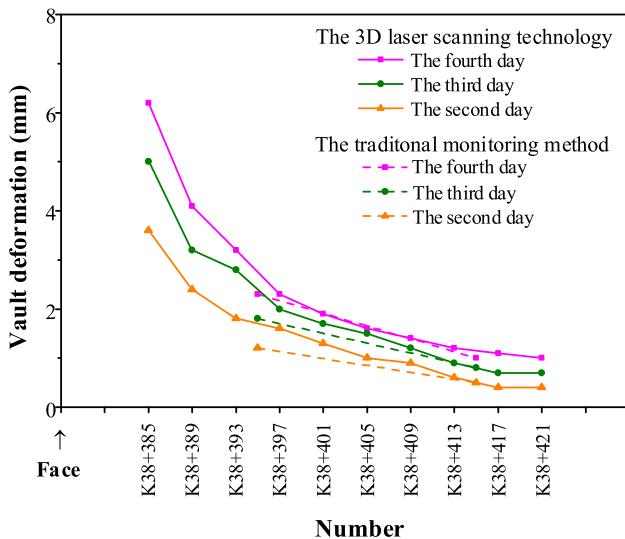

Fig. 17 Comparison between traditional method and 3D laser scanning method

this paper to improve the efficiency of ICP procedure while ensuring the precision of the data.

5 Conclusions

The 3D laser scanning technology is applied in the deformation monitoring of Nanshan tunnel, and a new data processing method is proposed in this paper. The following conclusions can be reached.

(1) The IMA method is proposed to reduce point cloud data. The results show that the method can maintain the accuracy rate at 78% when the reserved ratio is as low as 3%, which is significantly better than the RS method and the CS method.

(2) The calculation of the correspondence between multi-temporal point clouds by ICP algorithm is effective for the rough lining of NATM tunnel monitoring, which is verified by the 20 mm convergence test.

(3) The tunnel full-space deformation field is obtained, which provides extensive deformation information of the complete tunnel lining. The difference between traditional total station monitoring method and proposed method is less than 0.5 mm indicating a great agreement.

References

1. Becerik-Gerber B, Jazizadeh F, Kavulya G et al (2011) Assessment of target types and layouts in 3D laser scanning for registration accuracy. Autom Constr 20:649–658. https://doi.org/10.1016/j.autcon.2010.12.008

2. Besl P, McKay HD (1992) A method for registration of 3-D shapes. IEEE Trans Pattern Anal Mach Intell 14:239–256. https://doi.org/10.1109/34.121791

3. Carranza-Torres C, Fairhurst C (2000) Application of the Convergence-Confinement method of tunnel design to rock masses that satisfy the Hoek-Brown failure criterion. Tunn Undergr Space Technol 15:187–213. https://doi.org/10.1016/S0886-7798(00)00046-8

4. Chae BG, Ichikawa Y, Jeong GC et al (2004) Roughness measurement of rock discontinuities using a confocal laser scanning microscope and the Fourier spectral analysis. Eng Geol 72:181–199. https://doi.org/10.1016/j.enggeo.2003.08.002

5. Dehghan AN, Shafiee SM, Rezaei F (2012) 3-D stability analysis and design of the primary support of Karaj metro Tunnel: based on convergence data and back analysis algorithm. Eng Geol 141–142:141–149. https://doi.org/10.1016/j.enggeo.2012.05.008

6. Deng G, Cahill L (1993) An adaptive Gaussian filter for noise reduction and edge detection. In: 1993 IEEE conference record nuclear science symposium and medical imaging conference. IEEE, pp 1615–1619

7. Forest J, Salvi J (2002) A review of laser scanning three-dimensional digitisers. In: IEEE/RSJ international conference on intelligent robots and systems, vol 71, pp 73–78

8. Gikas V (2012) Three-dimensional laser scanning for geometry documentation and construction management of highway tunnels during excavation. Sensors (Basel) 12:11249–11270. https://doi.org/10.3390/s120811249

9. Gutiérrez F, Benito-Calvo A, Carbonel D et al (2019) Review on sinkhole monitoring and performance of remediation measures by high-precision leveling and terrestrial laser scanner in the salt karst of the Ebro Valley, Spain. Eng Geol 248:283–308. https://doi.org/10.1016/j.enggeo.2018.12.004

10. Han J-Y, Guo J, Jiang Y-S (2013) Monitoring tunnel profile by means of multi-epoch dispersed 3-D LiDAR point clouds. Tunn

Undergr Space Technol 33:186–192. https://doi.org/10.1016/j.tust.2012.08.008

11. Kolymbas D (2005) Tunnelling and tunnel mechanics: a rational approach to tunnelling. Springer Science, Business Media

12. Kontogianni VA, Stiros SC (2005) Induced deformation during tunnel excavation: evidence from geodetic monitoring. Eng Geol 79:115–126. https://doi.org/10.1016/j.enggeo.2004.10.012

13. Lindenbergh R, Pfeifer N, Rabbani T (2005) Accuracy analysis of the Leica HDS3000 and feasibility of tunnel deformation monitoring. In: Proceedings of the ISPRS workshop, Laser scanning, vol 3

14. Mitra NJ, Nguyen A (2003) Estimating surface normals in noisy point cloud data. In: Proceedings of the nineteenth annual symposium on computational geometry, pp 322–328

15. MOHURD (2014) Standard for engineering classification of rock mass (GB/T 50218–2014). Ministry of Housing and Urban-Rural Development of the People's Republic of China, Beijing, China

16. Mukupa W, Roberts GW, Hancock CM et al (2017) A review of the use of terrestrial laser scanning application for change detection and deformation monitoring of structures. Surv Rev 49:99–116. https://doi.org/10.1080/00396265.2015.1133039

17. Nuttens T, Stal C, De Backer H et al (2014) Methodology for the ovalization monitoring of newly built circular train tunnels based on laser scanning: Liefkenshoek Rail Link (Belgium). Autom Constr 43:1–9. https://doi.org/10.1016/j.autcon.2014.02.017

18. Sturzenegger M, Stead D (2009) Close-range terrestrial digital photogrammetry and terrestrial laser scanning for discontinuity characterization on rock cuts. Eng Geol 106:163–182. https://doi.org/10.1016/j.enggeo.2009.03.004

19. Teza G, Galgaro A, Zaltron N, Genevois R (2007) Terrestrial laser scanner to detect landslide displacement fields: a new approach. Int J Remote Sens 28:3425–3446. https://doi.org/10.1080/01431160601024234

20. Vendroux G, Knauss W (1998) Submicron deformation field measurements: Part 1. Developing a digital scanning tunneling microscope. Exp Mech 38:18–23

21. Wang W, Zhao W, Huang L, Vimarlund V et al (2014) Applications of terrestrial laser scanning for tunnels: a review. J Traffic Transp Eng 1:325–337. https://doi.org/10.1016/S2095-7564(15)30279-8

22. Xie X, Zeng C (2012) Non-destructive evaluation of shield tunnel condition using GPR and 3D laser scanning. In: 14th international conference on ground penetrating radar (GPR), 2012, pp 479–484

23. Xie X, Lu X (2017) Development of a 3D modeling algorithm for tunnel deformation monitoring based on terrestrial laser scanning. Undergr Space 2(1):16–29

24. Yang H, Omidalizarandi M, Xu X et al (2017) Terrestrial laser scanning technology for deformation monitoring and surface modeling of arch structures. Compos Struct 169:173–179. https://doi.org/10.1016/j.compstruct.2016.10.095

25. Yue D, Wang J, Zhou J et al (2010) Monitoring slope deformation using a 3-D laser image scanning system: a case study. Min Sci Technol 20:898–903. https://doi.org/10.1016/s1674-5264(09)60303-3

26. Zinßer T, Schmidt J, Niemann H (2003) A refined ICP algorithm for robust 3-D correspondence estimation. In: Proceedings 2003 international conference on image processing (Cat. No. 03CH37429). IEEE, II-695